Efficient Curvature Analysis of Buried Waveguides

Phillip D. Sewell, *Member, IEEE,* and T. M. Benson,

***Abstract*—The highly efficient free space radiation mode method is extended, enabling for the first time its use in determining the lossy modes of curved buried semiconductor waveguides. Both the real and imaginary parts of the propagation constant along with the corresponding field profiles, are found with an accuracy comparable to that of more computationally intensive methods.**

I. Introduction

CURVED waveguides are an essential ingredient of modern integrated optoelectronics and therefore design tools that can accurately predict their field properties are of significant interest. In particular, precise determination of their modal properties, including the bending losses, is highly desirable. Thus, many approaches have applied to this problem over the years. These range from perturbations of straight waveguide solutions and simple asymptotic approximations for the curvature loss, through to full wave mode matching methods, and more numerical techniques such as the finite difference method, the method of lines, and beam propagation methods, [1]–[17]. While the perturbation methods are useful for bends with large radii of curvature, recent demands for relatively tight and, hence, relatively lossy bends, has encouraged the use of the latter approaches which are more accurate and widely applicable. It is also noteworthy that one particular stimulation for the development of accurate *fully vectorial* methods is the recent interest in the polarization conversion properties of waveguide bends, both as a cause of performance degradation and as the basis of useful devices, [18], [19]. However, as it is known that this phenomenon is primarily associated with structures containing large refractive index contrasts, such as those found in deeply etched rib waveguides, there is a still a substantial role for advanced *polarized* analyzes to play, specifically the study of moderately tight bends in buried waveguides.

Semi-analytical methods are often an attractive prospect for the designer who wishes to investigate a wide variety of design possibilities as they can combine good accuracy with fast execution times. Many such methods are available for a range of practical components, although it is usual that each method is ideally suited to a particular class of problems. One such semi-analytical approach is the free space radiation mode (FSRM) method, [20]–[27], which has been successfully applied to problems involving structures that have a relatively small refractive index contrast transverse to the direction of propagation. This class of problem encompasses a wide range of useful devices, in particular those based upon buried semiconductor waveguides and Fig. 1(a)–(c) illustrate schematically some of the structures that can be analyzed. A modified FSRM method, referred to as the half space radiation mode (HSRM) method, [28], allows the analysis to be readily extended to buried waveguides in the presence of a strong transverse index discontinuity, such as might occur at a semiconductor-air boundary, [see Fig. 1(d)].

In the past few years, the FSRM approach has been applied as a mode solver, including the vector case, to the demanding problem of coated and angled laser facet reflectivity as well as a propagation method used to analyze the performance of spot size converters, [20]–[27]. In each case, the results produced by the FSRM method were of comparable accuracy to those produced by far more numerically intensive approaches but with a substantial saving in calculation time.

The FRSM approach is based upon one simple approximation. It is assumed that the fields in a guiding structure possessing a small refractive index contrast can be expressed as a superposition of the fields of the local guided modes along with a simple plane wave spectrum which models the radiation field. This plane wave spectrum is subsequently treated as if it exists in a uniform medium of refractive index n_{un}. Clearly, this assumption is valid as the index contrast tends to zero, although in practice it has been found to yield accurate results for differences of up to 10%. Furthermore, the method is relatively insensitive to the exact choice of n_{un}. In fact, although one can usually find a specific value for n_{un} that maximizes the accuracy of a particular type of analysis, such as a finding the modes of straight waveguides, [21], simply using the value of the cladding index generally yields very good results.

The efficiency of the FSRM method can be traced to the ease with which transverse junction problems are handled. Unlike the mode matching method for example, which upon enforcing the boundary conditions requires the solution of a moderately large number of linear equations, the FSRM method explicitly expresses the plane wave amplitudes on either side of the junction in terms of the Fourier transforms of the local guided modes. Subsequently, requiring that the *total* radiation field which is represented by this plane wave spectrum to be orthogonal to the local guided modes then yields either a determinental equation in the case of a mode solver, or else the guided mode scattering coefficients in the case of a facet problem.

This paper applies the FSRM method to finding the lossy modes of curved buried waveguides. Although the detailed discussion is limited to a buried waveguide of rectangular core cross section, the principle applies to any waveguide with low transverse index contrast. It is important to note that the method gains further advantage in the determination of lossy modes as it is does not require the use of an artificially truncated calculation space and therefore correctly models the truly open nature of the problem.

Manuscript received December 3, 1999; revised May 30, 2000.

The authors are with the School of Electrical and Electronic Engineering, University of Nottingham, University Park, Nottingham NG7 2RD, U.K.

Publisher Item Identifier S 0733-8724(00)08066-X.

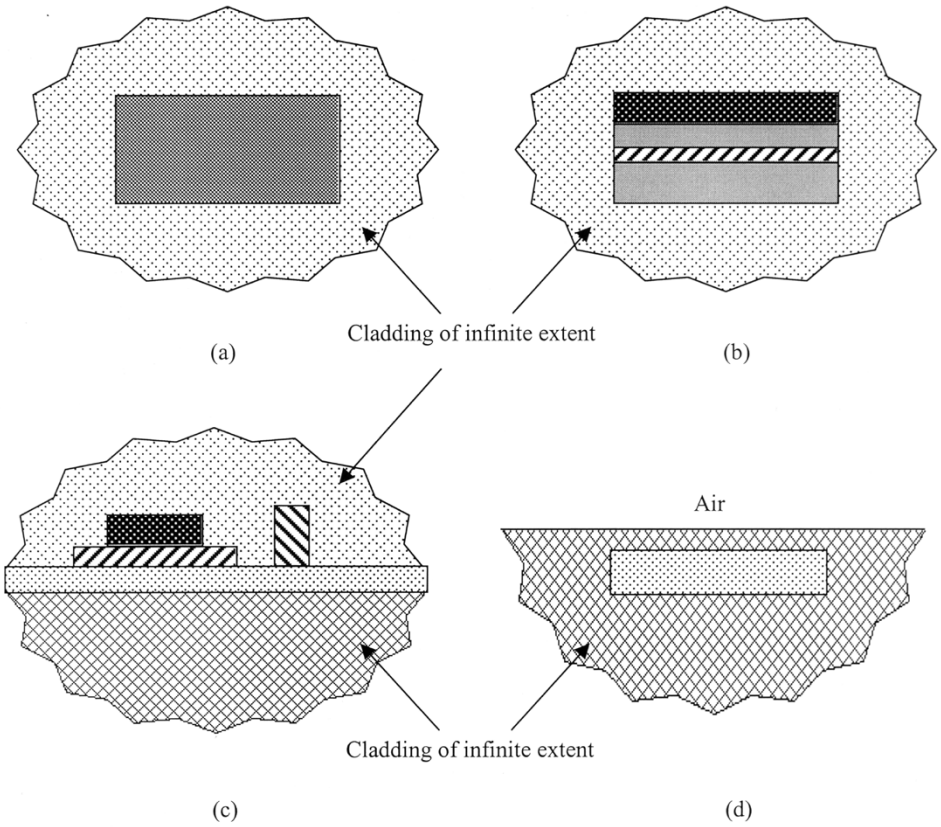

Fig. 1. (a)–(c) Schematic diagrams of buried structures which can be analyzed using the FSRM. (d) HSRM methods. (Note that all the refractive indexes, except that of the air in (d), must be within 10%) (a) Buried rectangular cores, [21], [22]. (b) Multilayer buried cores, for example, a double heterostructure laser [23]. (c) General buried guide structures, [23]. (d) Buried guides near to the air-semiconductor boundary [28].

II. Theory

The structure under consideration is shown in Fig. 2. The guide cross section consists of a core of refractive index n_c, height $2H$ and width $2W$, buried in a cladding material of index n_s. As discussed above, the FSRM approach is applicable when the index contrast between the core and the cladding is small, typically less than 10%. In such a case, the polarized approximation to the true vector field is a good one, [29], and the cross-polarization coupling that has been observed in air-semiconductor structures is negligible.

In this work, both scalar and five component polarized formulations have been developed. For transverse electric (TE) modes, the principal field components explicitly appearing in the analysis are H_y and E_θ and for transverse magnetic (TM) modes, E_y and H_θ.

Helmholtz's equation, conveniently expressed in cylindrical coordinates, requires that

$$\left[\frac{1}{r}\frac{\partial}{\partial r}r\frac{\partial}{\partial r}+\frac{\partial^2}{\partial^2 y}+k^2-\frac{\nu^2}{r^2}\right]H_y(r,y)e^{-j\nu\theta}=0$$

for the TE case and

$$\left[\frac{1}{r}\frac{\partial}{\partial r}r\frac{\partial}{\partial r}+\frac{\partial}{\partial y}\frac{1}{n^2}\frac{\partial n^2}{\partial y}+k^2-\frac{\nu^2}{r^2}\right]E_y(r,y)e^{-j\nu\theta}=0$$

for the TM case. (1)

Subsequently, φ will be used to represent either H_y (TE case) or E_y (TM case).

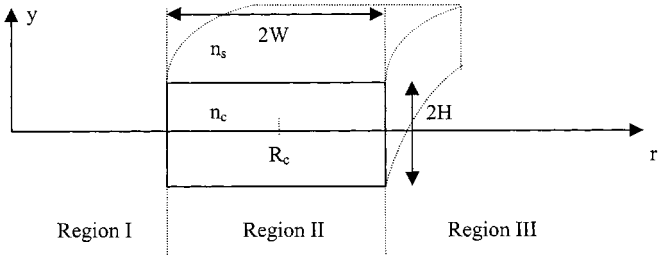

Fig. 2. The cross section of the curved buried rectangular waveguide.

The structure is divided into three regions as shown in Fig. 2. In regions I and III, the total field can be represented exactly as a superposition of plane waves and in region II the field is expressed as a superposition of the guided mode of a vertical three-layer slab and a radiation field. As discussed in the introduction, the radiation field is approximated by a plane wave spectrum assumed to exist in a uniform medium of refractive index n_{un}.

Consequently, we represent the field, φ as

Region I:

$$\varphi(r,y)=\int_0^\infty ds\sqrt{2/\pi}\cos(sy)\frac{J_\nu(\rho r)}{J_\nu(\rho r_1)}(\tilde{\phi}_g(s)A+\tilde{a}(s)). \quad (2)$$

Region II:

$$\begin{aligned}\varphi(r,\,y) &= \phi_g(y)\\ &\quad\cdot\left(\left[\frac{J_\nu(\gamma_g r)H_\nu^{(2)}(\gamma_g r_2)-H_\nu^{(2)}(\gamma_g r)J_\nu(\gamma_g r_2)}{J_\nu(\gamma_g r_1)H_\nu^{(2)}(\gamma_g r_2)-H_\nu^{(2)}(\gamma_g r_1)J_\nu(\gamma_g r_2)}\right]A\right.\\ &\quad\left.+\left[\frac{J_\nu(\gamma_g r)H_\nu^{(2)}(\gamma_g r_1)-H_\nu^{(2)}(\gamma_g r)J_\nu(\gamma_g r_1)}{J_\nu(\gamma_g r_1)H_\nu^{(2)}(\gamma_g r_2)-H_\nu^{(2)}(\gamma_g r_1)J_\nu(\gamma_g r_2)}\right]B\right)\\ &\quad+\int_0^\infty ds\sqrt{2/\pi}\,\cos(sy)\\ &\quad\cdot\left(\left[\frac{J_\nu(\gamma r)H_\nu^{(2)}(\gamma r_2)-H_\nu^{(2)}(\gamma r)J_\nu(\gamma r_2)}{J_\nu(\gamma r_1)H_\nu^{(2)}(\gamma r_2)-H_\nu^{(2)}(\gamma r_1)J_\nu(\gamma r_2)}\right]\tilde{a}(s)\right.\\ &\quad\left.+\left[\frac{J_\nu(\gamma r)H_\nu^{(2)}(\gamma r_1)-H_\nu^{(2)}(\gamma r)J_\nu(\gamma r_1)}{J_\nu(\gamma r_1)H_\nu^{(2)}(\gamma r_2)-H_\nu^{(2)}(\gamma r_1)J_\nu(\gamma r_2)}\right]\tilde{b}(s)\right).\end{aligned} \tag{3}$$

Region III:

$$\varphi(r,\,y)=\int_0^\infty ds\sqrt{2/\pi}\,\cos(sy)\frac{H_\nu^{(2)}(\rho r)}{H_\nu^{(2)}(\rho r_2)}(\tilde{\phi}_g(s)B+\tilde{b}(s)) \tag{4}$$

where

1) even symmetry has been assumed in the y direction;
2) γ_g is the propagation constant of the vertical three-layer slab mode in region II;
3) $\phi_g(y)$ is the field profile of the vertical three-layer slab mode in region II, specifically represented below as $h_y(y)$ and $e_y(y)$ for the TE and TM cases respectively;
4) $\tilde{\phi}_g(s)$, and below $\tilde{h}_{yg}(s)$ and $\tilde{e}_{yg}(s)$, are the Fourier transforms of the field profiles of the three-layer slab mode;
5) $\gamma=\sqrt{k_{\rm un}^2-s^2}$ and $\rho=\sqrt{k_s^2-s^2}$;
6) $k_s=n_sk_o$, $k_c=n_ck_o$, $k_{\rm un}=n_{\rm un}k_o$;
7) $k_o=2/\pi$, λ being the free space wavelength;
8) A and B are constants and $\tilde{a}(s)$ and $\tilde{b}(s)$ are the spectral coefficients of the radiation field.

It is observed that at the edges of the guide, $r_1=r_c-W$ and $r_2=r_c+W$, the representation of the field in (2)–(4) is already continuous as required.

It is also necessary, to enforce continuity of E_θ in the TE case or H_θ in the TM case at $r=r_1$ and $r=r_2$. To enable this it is noted that for the plane waves;

$$\begin{aligned}\text{TE: } E_\theta &= \frac{j\omega\mu_o}{k_i^2-s^2}\,\frac{\partial H_y}{\partial r}\\ \text{TM: } H_\theta &= \frac{-j\omega n_i^2}{k_i^2-s^2}\,\frac{\partial E_y}{\partial r}\end{aligned} \tag{5}$$

where the subscript "i" indicates "s" for regions I and III and "un" for region II.

Similarly for the guided mode of the three-layer slab

$$\begin{aligned}\text{TE: } E_\theta &= \frac{j\omega\mu_o}{\gamma_g^2}\,\frac{\partial H_y}{\partial r}\\ \text{TM: } H_\theta &= \frac{-j\omega n_c^2}{\gamma_g^2}\,\frac{\partial E_y}{\partial r} \qquad \text{for } |y|<h\\ H_\theta &= \frac{-j\omega n_s^2}{\gamma_g^2}\,\frac{\partial E_y}{\partial r} \qquad \text{for } |y|>h.\end{aligned} \tag{6}$$

Taking the Fourier transform of (5) and (6) with respect to y, the continuity of H_θ is satisfied for the TE case if, in the transform space, as shown in (7) and (8) at the bottom of the page where $J_\nu'(z)$ denotes $(\partial J_\nu(z)/\partial z)$, etc.

Similarly, for the TM case, continuity of E_θ requires that, as shown in (9) and (10) at the bottom of the next page. Note that to avoid a convolution the transform $\tilde{h}_{\theta g}(s)$is calculated directly from (6) in the space domain rather than from $\tilde{e}_{\theta g}(s)$.

$$\begin{aligned}\frac{\tilde{h}_{yg}(s)A+\tilde{a}(s)}{\rho}\left(\frac{J_\nu'(\rho r_1)}{J_\nu(\rho r_1)}\right) &= \tilde{e}_{\theta g}(s)\gamma_g\frac{\left(J_\nu'(\gamma_g r_1)H_\nu^{(2)}(\gamma_g r_2)-H_\nu'^{(2)}(\gamma_g r_1)J_\nu(\gamma_g r_2)\right)A+\dfrac{2}{\pi\gamma_g r_1}B}{J_\nu(\gamma_g r_1)H_\nu^{(2)}(\gamma_g r_2)-H_\nu^{(2)}(\gamma_g r_1)J_\nu(\gamma_g r_2)}\\ &\quad+\frac{1}{\gamma}\,\frac{\left(J_\nu'(\gamma r_1)H_\nu^{(2)}(\gamma r_2)-H_\nu'^{(2)}(\gamma r_1)J_\nu(\gamma r_2)\right)\tilde{a}(s)+\dfrac{2}{\pi\gamma r_1}\tilde{b}(s)}{J_\nu(\gamma r_1)H_\nu^{(2)}(\gamma r_2)-H_\nu^{(2)}(\gamma r_1)J_\nu(\gamma r_2)}\end{aligned} \tag{7}$$

and

$$\begin{aligned}\frac{\tilde{h}_{yg}(s)B+\tilde{b}(s)}{\rho}\left(\frac{H_\nu'^{(2)}(\rho r_2)}{H_\nu^{(2)}(\rho r_2)}\right) &= \tilde{e}_{\theta g}(s)\gamma_g\frac{\dfrac{2}{\pi\gamma_g r_2}A+\left(J_\nu'(\gamma_g r_2)H_\nu^{(2)}(\gamma_g r_1)-H_\nu'^{(2)}(\gamma_g r_2)J_\nu(\gamma_g r_1)\right)B}{J_\nu(\gamma_g r_1)H_\nu^{(2)}(\gamma_g r_2)-H_\nu'^{(2)}(\gamma_g r_1)J_\nu(\gamma_g r_2)}\\ &\quad+\frac{1}{\gamma}\,\frac{\dfrac{2}{\pi\gamma r_2}\tilde{a}(s)+\left(J_\nu'(\gamma r_2)H_\nu^{(2)}(\gamma r_1)-H_\nu'^{(2)}(\gamma r_2)J_\nu(\gamma r_1)\right)\tilde{b}(s)}{J_\nu(\gamma r_1)H_\nu^{(2)}(\gamma r_2)-H_\nu^{(2)}(\gamma r_1)J_\nu(\gamma r_2)}.\end{aligned} \tag{8}$$

Equations (7) and (8) for the TE mode or (9) and (10) for the TM mode can now be straightforwardly rearranged to give

$$\begin{pmatrix} \tilde{a}(s) \\ \tilde{b}(s) \end{pmatrix} = \underline{\underline{\tilde{M}}}_{\nu}(s) \begin{pmatrix} A \\ B \end{pmatrix} \tag{11}$$

where $\underline{\underline{\tilde{M}}}_{\nu}(s)$ is a 2×2 matrix.

It is commented here that if the true radiation mode spectrum of the three-slab had been used rather than the FSRM approximation to it, then it would not have been possible to derive an explicit expression for the spectral coefficients as in (11). Rather an integral equation for the total fields at r_1 and r_2 would be obtained. Even if the discrete radiation modes of a boxed slab had been used, it would be necessary to solve a large set of linear equations to recover the spectral coefficients. Thus, it is (11) that is the key to the simplicity of the FSRM method.

The total FSRM radiation field, denoted below by the subscript "un," is now required to be orthogonal to the guided modes of the three-layer slab and this is enforced at both $r = r_1$ and $r = r_2$ in the form, [24],

$$\int_0^{\infty} dy[E_g^*(y, r) \times H_{\text{un}}(y, r) + E_{\text{un}}^*(y, r) \times H_g(y, r)].\hat{\theta} = 0 \tag{12}$$

This is conveniently evaluated in the transform space using (2)–(11) and for compactness the overall result is written in the form,

$$\int_0^{\infty} ds \underline{\underline{N}}_{\nu}(s) \begin{pmatrix} A \\ B \end{pmatrix} = \begin{pmatrix} 0 \\ 0 \end{pmatrix} \tag{13}$$

The modes of the buried guide are characterized by the values of ν which reduce the determinant of the 2×2 matrix $\int_0^{\infty} ds \underline{\underline{N}}_{\nu}(s)$ to 0 and the fields are then given by (2), (3), (4), (6) and (11).

There exist a number of straightforward extensions to the basic approach which increase its flexibility.

1) A vectorial formulation of this analysis is also possible if deemed necessary by combining the above procedure with the vectorial approach of [22], however this is not required for many examples of buried waveguide structures with low transverse refractive index contrast such as those presented below.
2) A further extension that may be appropriate occurs when the vertical three-layer slab of region II supports more than one guided mode. In this case the analysis is modified in a manner similar to that presented in [25] for the case of propagation in straight guides. In this circumstance, the simple constants A and B above become vectors and the orthogonality between the FSRM radiation field and each local guided slab mode is imposed separately. This yields a matrix equivalent to N_{ν} in (13) whose order is twice the number of guided modes supported by the slab.
3) The case of diffused channel waveguides, which have a small index contrast between the channel and substrate but a large contrast between the guide and the air above [see Fig. 1(d)], can be dealt with by combining the following approach with the HSRM method described in [28].
4) Finally, more complex structures such as that shown in Fig. 1(c) can be tackled in a manner similar to that presented in [23]. In each of the regions supporting guided slab modes, (analogous to region II of Fig. 2), an expansion like that of (3) is available and continuity between the regions is sufficient to determine the FSRM spectral coefficients in each. Again, application of the orthogonality requirement in each region yields an equation equivalent to (13).

The practical implementation of the approach presented here is simple in practice. However, as is well known, care needs to be taken to ensure sufficiently accurate evaluation the Bessel functions of complex order. In this work we have used the uniform asymptotic expansions for these as well as for the neces-

$$\frac{\tilde{c}_{yg}(s)A + n_s^2\tilde{a}(s)}{\rho} \begin{pmatrix} J_{\nu}'(\rho r_1) \\ J_{\nu}(\rho r_1) \end{pmatrix} = \tilde{h}_{\theta g}(s)\gamma_g \frac{\left(J_{\nu}'(\gamma_g r_1)H_{\nu}^{(2)}(\gamma_g r_2) - H_{\nu}'^{(2)}(\gamma_g r_1)J_{\nu}(\gamma_g r_2)\right)A + \dfrac{2}{\pi\gamma_g r_1}B}{J_{\nu}(\gamma_g r_1)H_{\nu}^{(2)}(\gamma_g r_2) - H_{\nu}^{(2)}(\gamma_g r_1)J_{\nu}(\gamma_g r_2)}$$
$$+ \frac{n_u^2}{\gamma} \frac{\left(J_{\nu}'(\gamma r_1)H_{\nu}^{(2)}(\gamma r_2) - H_{\nu}'^{(2)}(\gamma r_1)J_{\nu}(\gamma r_2)\right)\tilde{a}(s) + \dfrac{2}{\pi\gamma r_1}\tilde{b}(s)}{J_{\nu}(\gamma r_1)H_{\nu}^{(2)}(\gamma r_2) - H_{\nu}^{(2)}(\gamma r_1)J_{\nu}(\gamma r_2)} \tag{9}$$

and

$$\frac{\tilde{c}_{yg}(s)B + n_s^2\tilde{b}(s)}{\rho} \begin{pmatrix} H_{\nu}'^{(2)}(\rho r_2) \\ H_{\nu}^{(2)}(\rho r_2) \end{pmatrix} = \tilde{h}_{\theta g}(s)\gamma_g \frac{\dfrac{2}{\pi\gamma_g r_2}A + \left(J_{\nu}'(\gamma_g r_2)H_{\nu}^{(2)}(\gamma_g r_1) - H_{\nu}'^{(2)}(\gamma_g r_2)J_{\nu}(\gamma_g r_1)\right)B}{J_{\nu}(\gamma_g r_1)H_{\nu}^{(2)}(\gamma_g r_2) - H_{\nu}'^{(2)}(\gamma_g r_1)J_{\nu}(\gamma_g r_2)}$$
$$+ \frac{n_u^2}{\gamma} \frac{\dfrac{2}{\pi\gamma r_2}\tilde{a}(s) + \left(J_{\nu}'(\gamma r_2)H_{\nu}^{(2)}(\gamma r_1) - H_{\nu}'^{(2)}(\gamma r_2)J_{\nu}(\gamma r_1)\right)\tilde{b}(s)}{J_{\nu}(\gamma r_1)H_{\nu}^{(2)}(\gamma r_2) - H_{\nu}^{(2)}(\gamma r_1)J_{\nu}(\gamma r_2)}. \tag{10}$$

TABLE I
THE MODAL PARAMETERS OF THE FUNDAMENTAL (A) TE AND (B) TM MODES. $\lambda = 1.55\ \mu$m, $2W = 6\ \mu$m, $2H = 3\ \mu$m, $n_s = 1.50$ AND $n_c = 1.52$. (FREE SPACE RADIATION MODE METHOD, FSRM, SOURCE TYPE INTEGRAL METHOD, STIM, METHOD OF LINES, MoL, SEMI-VECTORIAL FINITE DIFFERENCE, SVFD AND EFFECTIVE INDEX, EI)

TE_{00}

	n_{eff}					L_{rad}				
$(R_c+W)/\lambda$	STIM[12]	MoL[12]	EIM[12]	SVFD	FSRM	STIM[12]	MoL[12]	EIM[12]	SVFD	FSRM
800	1.5068269	1.5068216	1.5071128	1.506836	1.5068253	0.3689	0.3635	0.7837	0.3656	0.3683
700	1.5064572	1.5064507	1.5067771	1.506467	1.5064556	0.8541	0.8421	1.7131	0.8506	0.8528
600	1.5059981	1.5059887	1.5063663	1.506008	1.5059958	1.9097	1.8844	3.5774	1.901	1.9073
500	1.5054095	1.5053956	1.5058465	1.505410	1.5054065	4.0816	4.0317	7.0747	4.053	4.0777
400	1.5046160	1.5045934	1.5051494	1.504617	1.5046120	8.2558	8.1663	13.172	8.221	8.2516
300	1.5034476	1.5033661	1.5041183	1.503454	1.5034428	15.694	15.549	23.047	15.66	15.696

(a)

TM_{00}

	n_{eff}					L_{rad}				
$(R_c+W)/\lambda$	STIM[12]	MoL[12]	EIM[12]	SVFD	FSRM	STIM[12]	MoL[12]	EIM[12]	SVFD	FSRM
800	1.5067611	1.5067598	1.5070402	1.506768	1.5067602	0.3958	0.3887	0.8393	0.3925	0.3952
700	1.5063941	1.5063911	1.5067067	1.506402	1.5063931	0.9054	0.8901	1.8111	0.9048	0.9039
600	1.5059382	1.5059322	1.5062986	1.505947	1.5059360	2.0003	1.9692	3.7348	2.006	1.9978
500	1.5053538	1.5053433	1.5057817	1.505365	1.5053510	4.2246	4.1659	7.2986	4.243	4.2209
400	1.5045658	1.5045465	1.5050878	1.504569	1.5045618	8.4483	8.3468	13.442	8.382	8.4450
300	1.5034044	1.5033661	1.5040591	1.503415	1.5034001	15.890	15.731	23.290	15.91	15.896

(b)

sary Airy functions since although they are more complicated than the Debye expansions, they are more generally applicable, [11], [31].

III. RESULTS

In order to validate the accuracy of the extended FSRM approach, we will first compare the results obtained with results from other methods which have been reported in the literature. Furthermore, we have also produced results from a polarized (semivectorial) finite difference (SVFD) mode solver, implemented in cylindrical coordinates and using perfectly matched layers as absorbing boundaries, [32].

The first example has core and cladding indexes of 1.52 and 1.50, respectively, $\lambda = 1.50\ \mu$m, $2H = 3.0\ \mu$m and $2W = 6\ \mu$m. Results are presented in Table I for the effective index, n_{eff}, which to be consistent with [12] is defined as $(\text{Re}(\nu)/k_o(R_c + W))$, and $L_{\text{rad}} = -10\pi\text{Im}(\nu)/\ln(10)$, the curvature loss for a 90° bend. It is noted that the results from the method of lines, (MoLs) and the source type integral equation method (STIM) taken from [12] are in fact vectorial.

From Table I(a) and (b) it is immediately apparent that there is excellent agreement between the FSRM results and those from the other methods. To emphasize this, Fig. 3(a) and (b) plot the percentage difference between the results from each method and the STIM. To allow close scrutiny, this has been done for the real part of propagation constant using the more sensitive normalized quantity

$$b = \frac{[\text{Re}(n_{\text{eff}})]^2 - n_s^2}{n_c^2 - n_s^2}$$

It is seen that the agreement with the STIM is especially good for both TE and TM cases which not only confirms the accuracy of the FSRM approach, but also validates the use of polarized fields for this example. Finally, it is clear that the simple effective index (EI) method is inadequate for this example, particularly in predicting the bending loss. However, it is interesting to observe that the FSRM analysis reduces to the EI method if one neglects the radiation fields in the core region, although their inclusion for this problem is clearly necessary.

Fig. 4 shows a selection of field profiles produced by the FSRM approach which not only clearly demonstrate the expected mode distortion caused by the bending, but also that the required field continuity is achieved.

To produce the results for the preceding example, n_s has been used as the uniform index of the FSRM radiation field in region II. The integration appearing in (12) is performed numerically, and convergence with both the upper limit and number of sample points confirmed. The overall calculation time depends upon the search algorithm used to identify the zeros of (13); the EI method can be used to identify a suitable initial estimate which is then refined using a standard zero search routine, [30]. Typically, calculation of each point on the curves using the FSRM method requires less than 20 s on a 600-MHz Pentium III PC for convergence to the accuracy presented here. In comparison, some of the SVFD results required substantially longer to compute. The fastest SVFD calculation times were found to be possible by using direct matrix techniques as opposed to iterative ones, although this required substantial quantities of memory. Typically on a 550-MHz alpha workstation the calculation time per point using the SVFD method could be brought down to no more than 20 min although this required about 200 MB of memory (using a mesh of 280 × 120 points and taking advantage of symmetry). It is also worth recalling that as described above, the complex order Bessel functions required by the FSRM method have been evaluated with the emphasis on accuracy rather than speed and it is possible that faster operation could be obtained by careful use of the

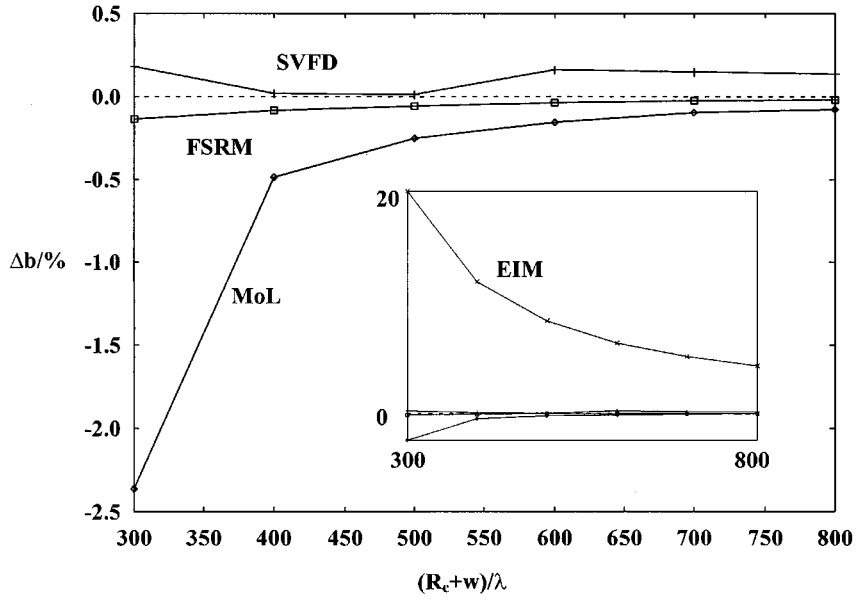

(a)

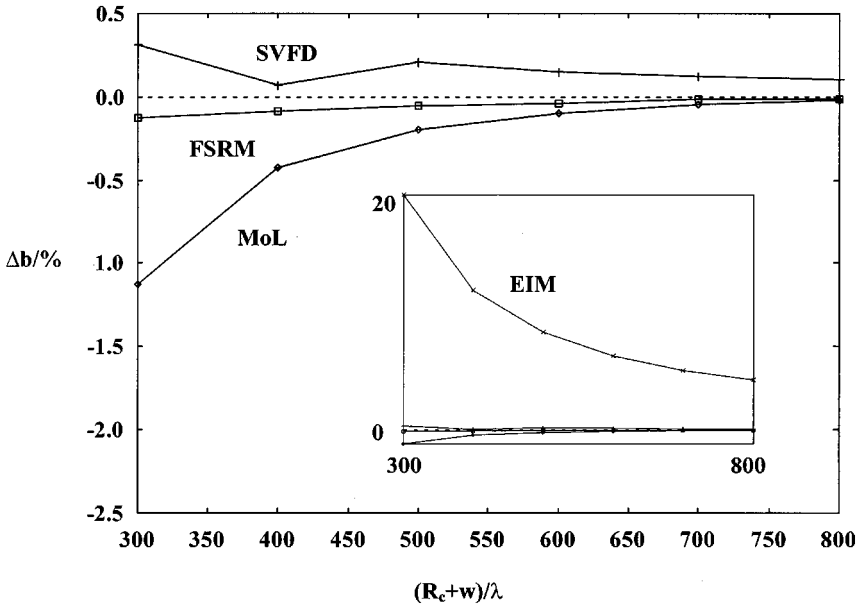

(b)

Fig. 3. Comparison of the normalized real part of the propagation constant of the fundamental (a) TE and (b) TM modes. $\lambda = 1.55\ \mu$m, $2W = 6\ \mu$m, $2H = 3\ \mu$m, $n_s = 1.50$ and $n_c = 1.52$. $\Delta b = (b - b_{\mathrm{STIM}})/b_{\mathrm{STIM}}$. $b = ([\mathrm{Re}(n_{\mathrm{eff}})]^2 - n_s^2)/(n_c^2 - n_s^2)$.

faster Debye expansions without compromising the overall accuracy. Notwithstanding this, the FSRM clearly provides a fast, yet precise tool for the purpose of practical design.

Having established the accuracy and speed of the FSRM approach, it is appropriate to investigate its range of validity and thus the refractive index difference between the core and the cladding regions of the waveguide was increased. In order to try to distinguish between the consequences of this index difference and other influences on the accuracy of the results, the height and width of the core were simultaneously varied so as to keep the normalized quantity $V = (2\pi/\lambda)H\sqrt{n_c^2 - n_s^2}$ constant with $W = 2H$. Furthermore, the radius of curvature was changed in each case to ensure that the radiation loss remained approximately the same for each example. These steps ensure that any variations in the accuracy with which the Bessel functions are evaluated for different arguments are minimized. Results are given in Table II for the both the real parts of the propagation constants and the radiation loss, noting that in this case the more straightforward definition of $n_{\mathrm{eff}} = (\mathrm{Re}(\nu)/k_o R_c)$ has been used. Moreover, Fig. 5 again shows the variation of the more sensitive parameter b. It can be seen that the agreement remains very good until Δn, defined as $(n_c - n_s)/n_s$, reaches about 10% and even at this point, the error is increasing only relatively slowly. Finally, it is appropriate to note that the results given in Table II and Fig. 5 are all for polarized case and for larger refractive index contrasts, attention will need to be given to the onset of fully vectorial behavior. As discussed above, this would be based upon the formulation presented in [22].

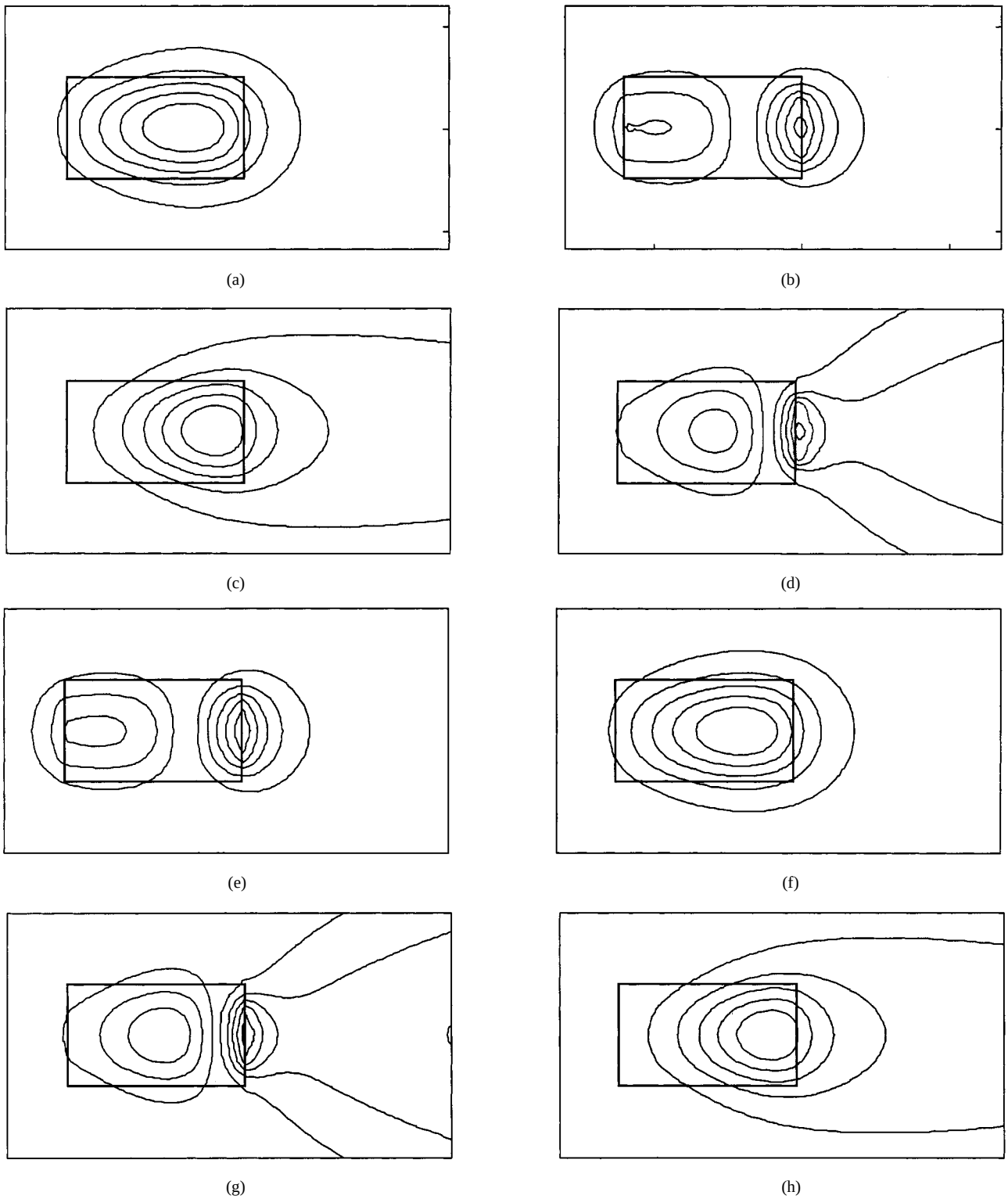

Fig. 4. Field plots for the structure of Fig. 3: (a) $|H_y|: TE,\ R_c + W = 1200\,\mu$m, (b) $|E_\theta|: TE,\ R_c + W = 1200\,\mu$m, (c) $|H_y|: TE,\ R_c + W = 450\,\mu$m, (d)$|E_\theta|: TE,\ R_c + W = 450\,\mu$m, (e) $|E_y|: TM,\ R_c + W = 1200\,\mu$m, (f) $|H_\theta|: TM,\ R_c + W = 1200\,\mu$m, (g) $|E_y|: TM,\ R_c + W = 450\,\mu$m, (h)$|H_\theta|: TM,\ R_c + W = 450\,\mu$m.

The final issue that is addressed is the choice of the background refractive index, n_{un}, in which the radiation fields in the waveguide core are assumed to exist. As discussed in the introduction, choosing $n_{\mathrm{un}} = n_s$ has previously proved a reliable selection, although to date, there does not exist a completely rigorous justification for doing so. However, to assess the sensitivity of the present analysis to the exact value used, Fig. 6 shows the change in modal parameters caused by varying n_{un}. The shaded bands on the figure show the spread in results obtained from STIM, MoL and SVFD, using $n_{\mathrm{eff}} = (\mathrm{Re}(\nu)/k_o R_c)$, and are used to gauge the sensitivity. It is clear that as claimed previously, the sensitivity to the exact value of n_{un} is not a problem.

TABLE II
THE MODAL PARAMETERS OF THE FUNDAMENTAL TE AND TM MODES. $\lambda = 1.55\ \mu$m, $(W/3) = \sqrt{(1.52^2 - n_s^2)/(n_c^2 - n_s^2)}$, $H = 2W$, $n_s = 1.50$ AND $\Delta n = (n_c - n_s/n_s)$

		TE_{00}				TM_{00}			
		n_{eff}		L_{rad}		n_{eff}		L_{rad}	
$\Delta n/\%$ (W/μm)	R_c/μm	FSRM	SVFD	FSRM	SVFD	FSRM	SVFD	FSRM	SVFD
1.51 (3.00)	1197	1.5106018	1.510610	0.3683	0.3655	1.5105365	1.510544	0.3952	0.3925
2.98 (2.00)	350	1.5237226	1.523761	0.2889	0.2861	1.5234012	1.523425	0.3358	0.3206
5.23 (1.50)	150	1.5416967	1.541846	0.2157	0.2204	1.5407151	1.540823	0.2803	0.2718
7.45 (1.25)	85	1.5596174	1.559894	0.2265	0.2186	1.5576683	1.557928	0.3217	0.3165
10.4 (1.05)	50	1.5835539	1.581920	0.2248	0.2323	1.5798153	1.578297	0.3582	0.3723

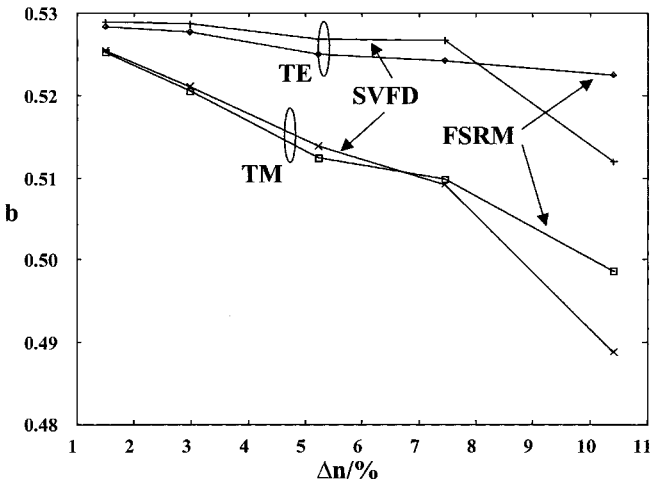

Fig. 5. Variation of the normalized real part of the propagation constant of the fundamental TE and TM modes with refractive index contrast, $\Delta n = (n_c - n_s/n_s)$. $\lambda = 1.55\ \mu$m, $W = 2 * H$ and $n_s = 1.50$, $b = ([\mathrm{Re}(n_{\mathrm{eff}})]^2 - n_s^2/n_c^2 - n_s^2)$ and $3\sqrt{1.52^2 - n_s^2} = H\sqrt{n_c^2 - n_s^2}$.

However, it is added that for values of n_{un} above about 1.51, rapid fluctuations do start to occur which are attributable to unphysical resonances of the FSRM radiation fields in the core. Therefore values of n_{un} which allow such resonances to occur should not be considered and we conclude that the practice of using $n_{\mathrm{un}} = n_s$ is a robust, albeit currently empirical, choice.

IV. CONCLUSION

A novel semi-analytical analysis of buried semiconductor waveguide bends has been presented. The method, based upon the FSRM approach, has been shown to provide highly accurate results requiring a short calculation time and minimal memory resources. Excellent agreement has been obtained between the results of this method and those from more numerically intensive "exact" techniques for the polarized solutions of relatively tightly curved structures. Full field profiles have also been presented. The extension of the approach to more geometrically complicated structures has been discussed as well as results demonstrating the range of validity of the method and the sensitivity to changes in the background index assumed in the model.

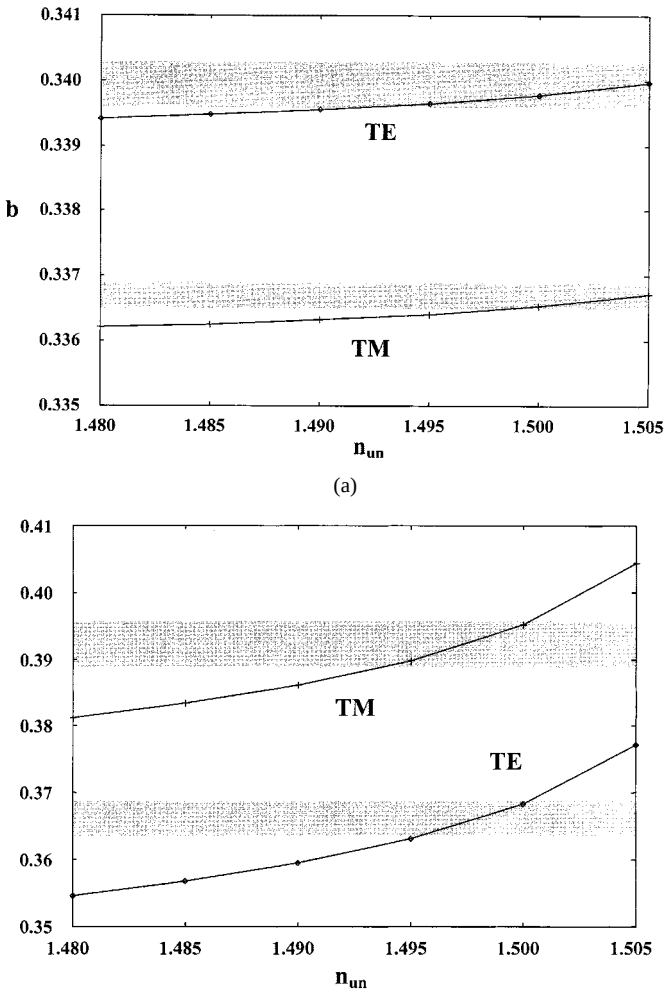

Fig. 6. Variation of the normalized real part of the propagation constant of the fundamental TE and TM modes with background index n_{un}. $\lambda = 1.55\ \mu$m, $2W = 6\ \mu$m, $2H = 3\ \mu$m, $(R_c + W)/\lambda = 800$, $ns = 1.50$ and $n_c = 1.52$. $b = ([\mathrm{Re}(n_{\mathrm{eff}})]^2 - n_s^2)/(n_c^2 - n_s^2)$. The shaded bands indicate the spread of values obtained from STIM, MoL and SVFD given in Table I.

REFERENCES

[1] E. A. J. Marcatili, "Bends in optical dielectric guides," *Bell Syst. Tech. J*, vol. 48, pp. 2103–2134, 1969.
[2] L. Lewin, "Radation from curved dielectric slabs and fibers," *IEEE Trans. Microwave Theory Tech.*, vol. 22, pp. 718–727, July 1974.
[3] P. C. Kendall, P. N. Robson, and J. E. Stitch, "Rib waveguide curvature loss: The scalar problem," *IEE Proc.*, pt. J, vol. 132, pp. 140–145, April 1985.
[4] T. Rozzi, G. Cerri, F. Chiaraluce, R. De Leo, and R. Ormondroyd, "Finite curvature and corrugations in dielectric ridge waveguides," *IEEE Trans. Microwave Theory Tech.*, vol. 36, pp. 68–79, Jan. 1988.

[5] S. J. Garth, "Mode behavior on bent planar dielectric waveguides," *Inst. Elec. Eng. Proc. Optoelectron.*, vol. 142, pp. 115–120, April 1995.
[6] A. Kumar, R. Jindal, and R. Gallawa, "Bending induced phase shifts in arbitrarily bent rectangular-core dual-mode waveguides," *J. Lightwave Technol.*, vol. 14, pp. 196–201, Feb. 1996.
[7] I. C. Goyal, R. L. Gallawa, and A. K. Ghatak, "Bent planar waveguides and whispering gallery modes: A new method of analysis," *J. Lightwave Technol.*, vol. 8, pp. 768–774, May 1990.
[8] S. Kim and A. Gopinath, "Vector analysis of optical dielectric waveguide bends using finite-difference method," *J. Lightwave Technol.*, vol. 14, pp. 2085–2092, Sept. 1996.
[9] R. T. Deck, M. Mirkov, and B. G. Bagley, "Determination of bending losses in rectangular waveguides," *J. Lightwave Technol.*, vol. 16, pp. 1703–1715, Sept. 1998.
[10] J.-S. Gu, P.-A. Besse, and H. Melchior, "Method of lines for the analysis of the propagation characteristics of curved optical rib waveguides," *IEEE J. Quantum Electron.*, vol. 27, pp. 531–537, Mar. 1991.
[11] R. S. Burton and T. Schlesinger, "Comparative analysis of the method of lines for three-dimensional curved dielectric waveguides," *J. Lightwave Technol.*, vol. 14, pp. 209–216, Feb. 1996.
[12] H. J. M. Bastiaansen, J. M. van der Keur, and H. Blok, "Rigorous, full-vectorial source-type integral equation analysis of circularly curved channel waveguides," *IEEE Trans. Microwave Theory Tech.*, vol. 43, pp. 401–409, Feb. 1995.
[13] H. Deng, G. H. Jin, J. Harari, J. P. Vilcot, and D. Decoster, "Investigation of 3-D semivectorial finite difference beam propagation method for bent waveguides," *J. Lightwave Technol.*, vol. 16, pp. 915–922, May 1998.
[14] W. W. Lui, C.-L. Xu, T. Hirono, K. Yokoyama, and W. P. Huang, "Full-vectorial wave propagation in semiconductor optical bending waveguides and equivalent straight waveguide approximations," *J. Lightwave Technol.*, vol. 16, pp. 910–914, May 1998.
[15] M. Rivera, "A finite difference BPM analysis of bent dielectric waveguides," *J. Lightwave Technol.*, vol. 13, pp. 233–238, Feb. 1995.
[16] ——, "Comments on investigation of 3-D semivectorial finite difference beam propagation method for bent waveguides," *J. Lightwave Technol.*, vol. 17, pp. 1103–1104, June 1999.
[17] J. Saijonmaa and D. Yevick, "Beam propagation analysis of loss in bent optical waveguides and fibers," *J. Opt. Soc. Amer.*, vol. 73, pp. 1785–1791, Dec. 1983.
[18] W. W. Lui, T. Hirono, K. Yokoyama, and W. P. Huang, "Polarization rotation in semiconductor bending waveguides: A coupled mode theory formulation," *J. Lightwave Technol.*, vol. 16, pp. 929–936, May 1998.
[19] C. Van Dam, L. H. Spiekman, F. P. G. M. Van Ham, G. H. Groen, J. Heidrich, C. M. Weinert, and M. K. Smit, "Novel compact polarization convertors based on ultra short bends," *IEEE Photon. Technol. Lett.*, vol. 8, pp. 1346–1348, Oct. 1996.
[20] M. Reed, T. M. Benson, P. C. Kendall, and P. Sewell, "Antirefelction-coated angle facet design," *Inst. Elec. Eng. Proc. Optoelectron.*, vol. 143, pp. 214–220, Aug. 1996.
[21] M. Reed, T. M. Benson, P. Sewell, P. C. Kendall, G. M. Berry, and S. V. Dewar, "Free space radiation mode analysis of rectangular dielectric waveguides," *Opt. Quantum Electron.*, vol. 28, pp. 1175–1179, Sept. 1996.
[22] P. Sewell, T. M. Benson, M. Reed, P. C. , and P. C. Kendall, "Transcendental equation for the vectorial modes of buried optical waveguides," *IEEE Photon. Technol. Lett.*, pp. 70–72, Jan. 1997.
[23] P. Sewell, M. Reed, T. M. Benson, P. C. Kendall, and M. Noureddine, "Computationally efficient analysis of buried rectangular and rib waveguides with applications to semiconductor lasers," *Inst. Elec. Eng. Proc. Optoelectron.*, vol. 144, pp. 14–18, Feb. 1997.
[24] P. Sewell, M. Reed, T. M. Benson, and P. C. Kendall, "Full vector analysis of two dimensional angled and coated optical waveguide facets," *IEEE J. Quantum. Electron.*, vol. 33, pp. 2311–2318, Dec. 1997.
[25] M. Reed, P. Sewell, T. M. Benson, and P. C. Kendall, ""An efficient propagation algorithm for 3D optical waveguides," *Inst. Elec. Eng. Proc. Optoelectron.*, vol. 145, pp. 53–58, Feb. 1998.
[26] P. Sewell, "The free space radiation mode method," in *Photonics Devices for Telecommunications*. New York: Springer-Verlag, 1998, ch. 1.2.
[27] P. Sewell, T. M. Benson, and P. C. Kendall, "Efficient and accurate models of buried spot-size convertors," *Opt. Quantum Electron.*, vol. 31, pp. 909–925, 1999.
[28] A. Vukovic, P. Sewell, T. M. Benson, and P. C. Kendall, "Half space radiation mode method for buried waveguide analysis," *Opt. Quantum Electron.*, vol. 31, pp. 43–51, 1999.
[29] S. Sujecki, T. M. Benson, P. Sewell, and P. C. Kendall, "Novel vectorial analysis of optical waveguides," *J. Lightwave Technol.*, vol. 16, pp. 1329–1335, July 1998.
[30] W. H. Press, S. A. Teukolsky, W. T. Vetterling, and B. P. Flannery, *Numerical Recipies in C, the Art of Scientific Computing*, 2nd ed. Cambridge, U.K.: Cambridge University Press, 1992.
[31] M. Abramowitz and I. A. Stegun, *Handbook of Mathematical Functions*: National Bureau of Standards, June 1965.
[32] W. P. Huang, C. L. Xu, W. Lui, and K. Yokoyama, "The perfectly matched layer boundary condition for modal analysis of optical waveguides: Leaky mode calculations," *IEEE Photon. Technol. Lett*, vol. 8, pp. 652–654, May 1996.

Phillip D. Sewell (S'88–M'91), photograph and biography not available at the time of publication.

T. M. Benson (M'95), photograph and biography not available at the time of publication.